Modeling Bright Gamma-ray and Radio Emission from Fast Cloud Shocks at Middle-aged SNRs

Shiu-Hang (Herman) Lee
Japan Aerospace Exploration Agency, Sagamihara, Kanagawa, Japan

Daniel J. Patnaude, John C. Raymond, Patrick O. Slane
Harvard-Smithsonian Center for Astrophysics, Cambridge, MA 02138, U.S.A.

Shigehiro Nagataki
RIKEN Astrophysical Big Bang Laboratory, Wako, Saitama, Japan

Donald C. Ellison
North Carolina State University, Raleigh, NC 27695, U.S.A

February 22, 2016

Abstract

Recent observations by the Large Area Telescope (LAT) onboard the Fermi satellite have revealed bright gamma-ray emission from middle-aged supernova remnants (SNRs) inside our Galaxy. These remnants which also possess bright non-thermal radio shells are often found to be interacting directly with surrounding gas clouds. We explore the non-thermal emission mechanism at these dynamically evolved SNRs by constructing a hydrodynamical model. Two scenarios of particle acceleration, either a re-acceleration of Galactic cosmic rays (CRs) or an efficient nonlinear diffusive shock acceleration (NLDSA) of particles injected from downstream, are considered. Using parameters inferred from observations, our models are contrasted with the observed spectra of SNR W44. For the re-acceleration case, we predict a significant enhancement of radio and GeV emission as the SNR undergoes a transition into the radiative phase. If sufficiently strong magnetic turbulence is present in the molecular cloud, the re-acceleration scenario can explain the observed broadband spectral properties. The NLDSA scenario also succeeds in explaining the gamma-ray spectrum but fails to reproduce the radio spectral index. Efficient NLDSA also results in a significant post-shock CR pressure that limits the cooling compression and prevents the formation of a prominent dense shell. Some other interesting differences between the two models in hydrodynamical behavior and resulting spectral features are illustrated in detail.

1 Introduction

The *Fermi* Large Area Telescope (LAT) has surprised many of us by revealing that many middle-aged SNRs turn out to be bright gamma-ray emitters (e.g., Abdo et al. 2009, 2010a,b,c; Castro & Slane 2010). This implies that, despite their older dynamical ages, these SNRs can still manage to produce a appreciable amount of high-energy CRs up to at least a few tens of GeV in energies. The latest analysis of accumulated *Fermi* LAT data on the SNRs W44 and IC 443 by Ackermann et al. (2013) has clearly uncovered a kinematic cutoff at around 250 MeV in their γ-ray spectra, a signature spectral characteristic that strongly supports the hadronic origin of the γ-rays, thus providing a smoking gun evidence for the acceleration of protons at SNR shocks. Earlier measurements by *AGILE* have also shown similar evidences (Tavani et al. 2010; Giuliani et al. 2011). However, the observed bright γ-ray emission raises new challenges to conventional DSA theories of particle acceleration at collisionless shocks. First of all, these dynamically evolved remnants have slow shocks and hence are not normally

expected to be efficient particle accelerators like their younger cousins. Moreover, the observed γ-rays that are concentrated in the GeV energy band possess a peculiar spectral break in the underlying proton distribution, the origin of which is still not clearly understood.

Interestingly, the shocks of middle-aged SNRs are usually found to be propagating through high-density environments such as adjacent massive molecular clouds. Signatures like strong forbidden line emission around the shocks suggest that the shocks have undergone transition into the radiative phase. It is thus natural to question whether radiative shocks in molecular clouds can somehow manage to generate bright non-thermal radio and γ-ray emission with the observed properties. Uchiyama et al. (2010) proposed a scenario in which fast radiative J-shocks pick up and re-accelerate pre-existing CRs which are subsequently boosted further to higher energy density by compression inside a rapidly cooling and contracting shell behind the radiative shock. In this way, bright GeV γ-ray and radio synchrotron emission can be simultaneously produced to explain observations.

In this work, we investigate the immediate locality of a fast radiative cloud shocks and explore its broadband non-thermal emission mechanisms using a time-dependent hydrodynamical simulation, self-consistently coupled to an explicit treatment of DSA. This proceeding is a simplified version of Lee et al. (2015). Readers are referred to the full paper for further details omitted here.

2 Model

Our numerical calculations are performed using the *CR-hydro-NEI* simulation code (Lee et al. 2012). In our model, we consider a picture in which the progenitor star undergoes core-collapse and explodes into a tenuous wind cavity surrounded by a molecular cloud. The blastwave created by the expanding ejecta propagates into the cavity with high speed and eventually hits the interface with the surrounding dense medium (probably part of the parent molecular cloud of the progenitor star), typically at a radius ~ 10 pc from the explosion center (Chevalier 1999). It then drives a shock into the cloud (we will call it a 'cloud shock' hereafter) and keeps pushing through the dense medium, and eventually becomes radiative.

The molecular cloud is approximated as a uniform dense medium with a number density $n_0 = 200$ cm^{-3}. We trace the time evolution of the hydrodynamics of the cloud shock starting from the time of penetration, passing the point when the shock has decelerated to about 200 km s^{-1} and become fully radiative. Physics including particle acceleration through the diffusive shock acceleration (DSA) mechanism and microphysical processes such as ionization and recombination, thermal conduction, radiative cooling and photoionization heating are calculated simultaneously.

The fully time-dependent ionization and recombination of 12 chemical elements including H, He, C, N, O, Mg, Ne, Si, S, Ar, Ca and Fe are followed behind the shock. The details of our treatment of non-equilibrium ionization (NEI) can be found in Patnaude et al. (2009, 2010). By tracing the ionization states and number densities of all ion species in the post-shock plasma through the NEI calculation, we can compute their contributions to radiative cooling through various line and continuum emissions at each time step. However, we do not consider cooling and heating effects from molecular chemistry like molecule reformation and IR line emission below a few 100 K.

The elemental abundances in the dense cloud are taken from the observations and models of bright atomic lines from SNR molecular shocks in the IR band by Reach & Rho (2000). We adopt an instantaneous post-shock equilibration of temperatures among ions and electrons which has been implied to be realistic for slow SNR shocks (Ghavamian et al. 2001). The thermal conduction rate is taken to be 0.3 of the Spitzer rate for a coliisionless plasma.

The major contributions to the radio continuum and γ-ray emissions are synchrotron radiation emitted by primary (i.e., direct acceleration of thermal e^- or re-acceleration of pre-existing CR e^- and e^+) and secondary (i.e., e^- and e^+ from the decay of changed pions produced by hadronic interactions) leptons that gyrate around the post-shock B-field, and energetic γ-ray photons from the decay of neutral pions produced by the interaction of accelerated protons/ions with the dense gas around the shock, respectively. We consider two scenarios for particle acceleration: (1) re-acceleration of pre-existing high-energy particles by the cloud shock; (2) efficient acceleration of particles through

NLDSA via injection from the thermal pool behind the subshock.

The re-acceleration scenario involves the shock acceleration of pre-existing Galactic CRs, whose spectra in momentum space are $n_{p,\rm seed}(p) = 4\pi J_p \beta^{1.5} p^{-2.76}$ for protons with $p > 0.31$ GeVc^{-1} , and $n_{e,\rm seed}(p) = 4\pi J_e (1+p^2)^{-0.55} p^{-2}$ for electrons with $p > 0.02$ GeVc^{-1}. Here, $\beta \equiv v_i/c$ where v_i is the particle velocity. The normalization factors adopted are $J_p = 1.9$ cm^{-2}s^{-1}sr^{-1}GeV^{-1} and $J_e = 0.02$ cm^{-2}s^{-1}sr^{-1}GeV^{-1}, so the total energy densities of the seed protons and electrons are $\varepsilon_p \approx 0.81$ eV cm^{-3} and $\varepsilon_e \approx 4.8 \times 10^{-3}$ eV cm^{-3} respectively. We do not consider the acceleration of heavy ions or dust grains here.

It has been shown that strong magnetic turbulence is necessary to reproduce the observed γ-ray fluxes of middle-aged SNRs, which reduces the CR diffusion coefficient by a factor of ~ 100 relative to the Galactic mean (e.g., Fujita et al. 2009; Ohira et al. 2011; Yan et al. 2012). Therefore, for both acceleration scenarios, we consider a Bohm-like diffusion for the CRs, but only up to a certain particle momentum given by $p_{\rm br} = 10(T_0/10^4\ {\rm K})^{-0.4}(B_0/\mu{\rm G})^2 n_n^{-1} n_i^{-1/2} m_p c$ where n_n and n_i are the neutral and ion densities. Above $p_{\rm br}$, the ion-neutral damping effect in a partially neutral medium takes place (Malkov et al. 2011) since at the cloud shock, the upstream medium is expected to be partially ionized. The ion fraction $n_i/(n_i+n_n)$ in the precursor of the cloud shock can be estimated approximately from the current shock velocity $v_{\rm sk}$ using the results of Hollenbach & McKee (1989).

The maximum momentum $p_{\rm max}$ of the CR protons at the cloud shock is mostly determined by their escape far upstream. We model their escape through setting a free-escape-boundary (FEB) at 10% of the current shock radius ahead of the shock, so that CRs with diffusion lengths longer than the FEB in the precursor are considered to have escaped. The $p_{\rm max}$ of the CR electrons can be further limited by energy loss processes such as synchrotron and inverse-Compton losses if important.

Here and throughout this work, we adopt a distance $d_{\rm SNR} = 2.9$ kpc to the SNR, a final SNR radius $R_{\rm SNR} = 12.5$ pc, an ambient gas density $n_0 = 200$ cm^{-3}, magnetic field $B_0 = 25$ μG and pre-shock temperature $T_0 = 10^4$ K. The pre-shock density chosen is typical of the molecular shocks at SNR W44 which are most probably responsible for producing the bright radio synchrotron filaments (Yoshiike et al. 2013). We compare our results with available radio continuum (Castelletti et al. 2007; Sun et al. 2011; Planck Collaboration et al. 2014) and γ-ray data (Ackermann et al. 2013; Cardillo et al. 2014) of SNR W44.

3 Results

We first look at the general hydrodynamical behavior of a cloud shock just before and after its transition into the radiative phase. Figure 1 shows the time snapshots of the profiles of hydrodynamic variables for the re-acceleration case, including total gas density n, temperature T, magnetic field strength B and gas velocity v until the shock has just started to become radiative. Here, $t_{\rm tr} \equiv 2.9 \times 10^4 E_{51}^{4/17} n_0^{-9/17}$ yr is a characteristic timescale at which the transition to radiative phase takes place (Blondin et al. 1998). Here E_{51} is the total kinetic energy of the blastwave that drives the cloud shock in unit of 10^{51} erg. When the shock decelerates quickly with time in the dense medium and the post-shock gas temperature drops to around a few 10^5 K, radiative cooling becomes important. An enhancement of density and B-field with time due to rapid compression can be observed. A cool dense shell forms behind the shock which is pushed forward by a faster and hotter interior heated up earlier by a stronger shock in the past. In this phase, the dynamics approaches that of a pressure-driven blastwave. The cool shell is eventually dominated by and supported against further collapse by non-thermal pressures, as is known to be the case at radiative filaments in some remnants such as Cygnus Loop (Raymond et al. 1988).

Figure 2 shows the spectral evolution of the radio and γ-ray emission predicted by our model under the Galactic CR re-acceleration scenario. The corresponding evolution of integrated energy fluxes is also shown. The time variable t_c is counted from the moment the cloud shock is driven into the dense medium and is shown in units of $t_{\rm tr}$. At $t_c < 1.2\ t_{\rm tr}$, both the radio continuum and γ-ray flux increase gradually with time, as more re-accelerated CRs and secondary $e^{+/-}$ from pion decay accumulate downstream. Then, a prominent transition occurs at $t_c \approx 1.2\ t_{\rm tr}$ when the shock has

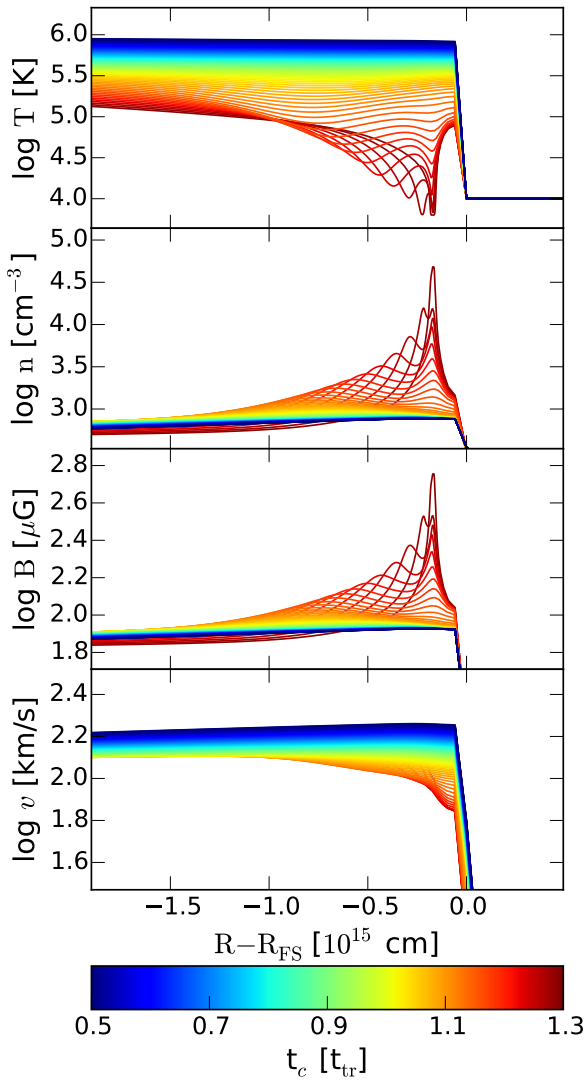

Figure 1: Time snapshots of profiles of hydrodynamic variables up to the stage when the shock has just become radiative for the re-acceleration model. From top to bottom: gas temperature, gas (proton) density, B-field strength and gas velocity. Radius is in units of the FS radius. The colorbar depicts the evolution age of the cloud shock in units of characteristic transition time $t_{\rm tr}$.

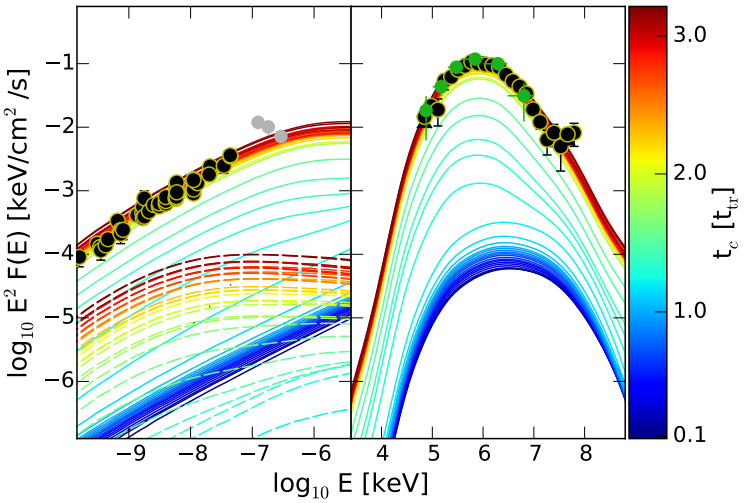

(a) Evolution of Broadband Spectrum

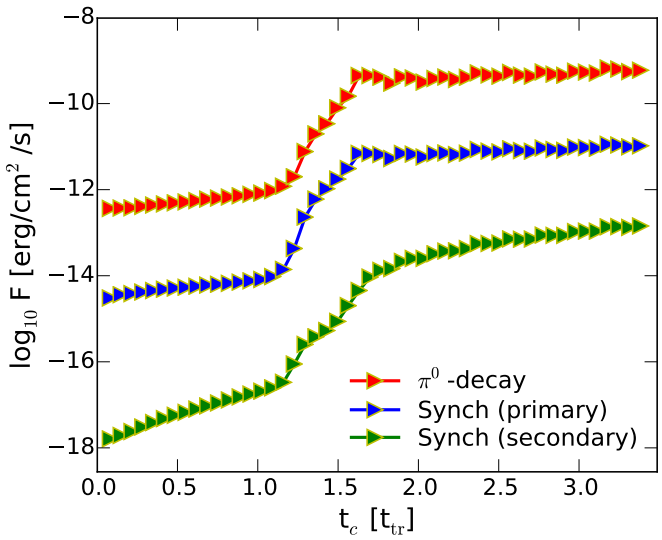

(b) Evolution of Integrated Flux

Figure 2: (a) Time evolution of the radio synchrotron (left panel) and π^0-decay γ-ray (right panel) spectra up to $t_c = 3\ t_{\rm tr}$ of our model under the Galactic CR re-acceleration scenario. Dashed lines in the left panel show the contribution from secondary e^- and e^+ to the synchrotron emission, while the solid lines show the total. Again, the colorbar depicts the evolution age of the cloud shock in units of $t_{\rm tr}$. The radio data points are scaled by a factor of 0.5. An overall normalization factor of 0.2 is applied to the model spectra to explain the data. (b) The corresponding evolution of the radio synchrotron and π^0-decay γ-ray flux. The energy ranges of flux integration for the radio and γ-ray photons are 70 MeV$-$20 GeV and 70 MHz$-$10 GHz respectively.

decelerated to a speed < 200 km s^{-1} whose dynamics start to be governed by radiative cooling. The compression of the B-field and gas density as well as the re-energization of the re-accelerated CRs and secondary particles in the rapidly cooling and contracting gas shell boost the non-thermal fluxes both in radio and γ-ray by a factor of a few 100. The spectral shape of the γ-rays also changes as the shock becomes slower than 120 km s^{-1} and experiences a partially ionized precursor so that the particle acceleration is hampered by the ion-neutral damping effect. Eventually, as the gas cools down and compresses, the non-thermal pressure becomes higher than the thermal pressure in the shell, and the cool shell is supported by the non-thermal pressure and stops contracting. We find an overall satisfactory agreement of the broadband spectral shape.

In this model, most of the bright π^0-decay γ-rays and radio synchrotron emission originate from the cool dense shell which is a thin compressed region behind the radiative cloud shock. This is qualitatively consistent with the filamentary morphology of the shell-like remnant revealed in the radio waveband. And as a result, the normalization of the non-thermal spectra for this model mainly depends on the compression of the cold dense shell, rather than the acceleration efficiency. To conform with the observed flux level, an overall normalization factor of 0.2 is applied to the model, which can be interpreted as a reasonable filling factor of the γ-ray and radio continuum emitting region over the whole 4π shell.

We do not show the detailed results for the second scenario in this proceeding, namely a NLDSA model with thermal injection mechanism. The results can be found in Lee et al. (2015). But in summary, we find a number of interesting differences with the re-acceleration model: (1) both the γ-ray and radio flux do not experience a boost after the transition of the shock to radiative phase, since the instantaneous efficiency of DSA is high during the early phase of the cloud shock evolution, resulting in a high non-thermal pressure that avoids rapid gas compression due to radiative cooling; (2) the shock becomes radiative at a much earlier time. The efficient DSA results into a lower post-shock temperature, thus speeding up the transition of the shock to its radiative phase; (3) the spectral index of the radio synchrotron emission is substantially steeper, failing to explain observation data. This model has a much more non-trivial time evolution of the shock compression ratio as well as the CR-driven amplification of B-field in the precursor, which are both quickly decreasing with time as the shock decelerates in the dense medium. Quickly DSA becomes inefficient as the shock evolves and the accelerated electrons possess a spectral index steeper than 2 in energy space. Consequently the overall electron spectrum is not hard enough to reproduce the observed radio index; (4) an overall normalization factor of 0.05 has to be applied to this model to reproduce the observed fluxes. This may not be easily attributable solely to the filling factor of the emission region. Since a prominent cool dense shell cannot be formed, the brightness profiles perpendicular to the shock front are also more diffuse and less filament-like than the former case, making this model less consistent with observation.

4 Conclusions

We explored the possibility of explaining the bright non-thermal radio and GeV emission from middle-aged SNRs through a scenario with re-acceleration of Galactic CRs or NLDSA of thermally injected particles by a fast radiative cloud shock. Using the *CR-hydro-NEI* code, we followed the hydrodynamics of a shock propagating in a gas cloud with a density typical of those found in GeV-bright middle-aged SNRs, and at the same time calculated the time evolution of the (re-)accelerated CRs in the downstream and the generation of associated broadband non-thermal emission.

In the re-acceleration scenario, we found that the transition of the cloud shock into the radiative phase, and the accompanying hydrodynamical effects on the post-shock conditions, play crucial roles in producing the bright non-thermal emission from the shell of these objects. The predicted general properties of the non-thermal emission agree well with observations and are illustrated by a comparison with the broadband spectrum of W44. As for the NLDSA scenario with 'thermal leakage' injection, a number of difficulties are found to explain observations. For example, the model fails to explain the radio continuum emission, with a spectral index too steep to reproduce typical observed values (e.g., W44 as well as others like IC 443 with similar indices).

We have limited our discussion in this paper to the study of general properties of non-thermal emission from a one-dimensional but time-evolving cloud shock with self-consistent DSA. While our model is far from a complete account of the rich observed properties of any particular middle-aged SNR owing to its one-dimensional nature, we believe it succeeds to capture the essence of the evolutionary behavior of a radiative cloud shock, and the expected non-thermal emission produced which to first order agrees with radio continuum and γ-ray observations. This model can be considered an important first step towards a fuller understanding of non-thermal emission from these objects.

References

Abdo, A. A., Ackermann, M., Ajello, M., et al. 2010a, ApJ, 718, 348

Abdo, A. A., Ackermann, M., Ajello, M., et al. 2009, ApJL, 706, L1

Abdo, A. A., Ackermann, M., Ajello, M., et al. 2010b, Science, 327, 1103

Abdo, A. A., Ackermann, M., Ajello, M., et al. 2010c, ApJ, 712, 459

Ackermann, M., Ajello, M., Allafort, A., et al. 2013, Science, 339, 807

Blondin, J. M., Wright, E. B., Borkowski, K. J., & Reynolds, S. P. 1998, ApJ, 500, 342

Cardillo, M., Tavani, M., Giuliani, A., et al. 2014, A&A, 565, A74

Castelletti, G., Dubner, G., Brogan, C., & Kassim, N. E. 2007, A&A, 471, 537

Castro, D. & Slane, P. 2010, ApJ, 717, 372

Chevalier, R. A. 1999, ApJ, 511, 798

Fujita, Y., Ohira, Y., Tanaka, S. J., & Takahara, F. 2009, ApJL, 707, L179

Ghavamian, P., Raymond, J., Smith, R. C., & Hartigan, P. 2001, ApJ, 547, 995

Giuliani, A., Cardillo, M., Tavani, M., et al. 2011, ApJ, 742, L30

Hollenbach, D. & McKee, C. F. 1989, ApJ, 342, 306

Lee, S.-H., Ellison, D. C., & Nagataki, S. 2012, ApJ, 750, 156

Lee, S.-H., Patnaude, D. J., Raymond, J. C., et al. 2015, ApJ, 806, 71

Malkov, M. A., Diamond, P. H., & Sagdeev, R. Z. 2011, Nature Communications, 2

Ohira, Y., Murase, K., & Yamazaki, R. 2011, MNRAS, 410, 1577

Patnaude, D. J., Ellison, D. C., & Slane, P. 2009, ApJ, 696, 1956

Patnaude, D. J., Slane, P., Raymond, J. C., & Ellison, D. C. 2010, ApJ, 725, 1476

Planck Collaboration, Arnaud, M., Ashdown, M., et al. 2014, ArXiv e-prints: 1409.5746

Raymond, J. C., Hester, J. J., Cox, D., et al. 1988, ApJ, 324, 869

Reach, W. T. & Rho, J. 2000, ApJ, 544, 843

Sun, X. H., Reich, P., Reich, W., et al. 2011, A&A, 536, A83

Tavani, M., Giuliani, A., Chen, A. W., et al. 2010, ApJ, 710, L151

Uchiyama, Y., Blandford, R. D., Funk, S., Tajima, H., & Tanaka, T. 2010, ApJL, 723, L122

Yan, H., Lazarian, A., & Schlickeiser, R. 2012, ApJ, 745, 140

Yoshiike, S., Fukuda, T., Sano, H., et al. 2013, ApJ, 768, 179